Journal of Applied Electrochemistry **34**: 159–168, 2004.

Electrochemical impedance spectroscopy of the alkaline manganese dioxide electrode

SCOTT W. DONNE[1,*] and JOHN H. KENNEDY[2]
[1]*Eveready Battery Company, Inc., 25225 Detroit Road, Westlake, OH 44145, USA*
[2]*Department of Chemistry, University of California, Santa Barbara, Santa Barbara, CA 93106, USA*
*(*author for correspondence, e-mail: scott.donne@newcastle.edu.au)*

Received 20 May 2003; accepted in revised form 2 September 2003

Key words: aqueous batteries, battery materials, electrochemical impedance spectroscopy, manganese dioxide

Abstract

Two-probe electrochemical impedance spectroscopy measurements were carried out on the electrolytic manganese dioxide electrode in concentrated KOH electrolytes under a variety of experimental conditions. These included varying the electrode thickness and compaction pressure, electrolyte content and concentration, degree of manganese dioxide reduction and the presence of TiO_2 (anatase) as an additive. The overall electrode impedance was found to decrease when thin electrodes, prepared under high compaction pressures, with an excess of electrolyte, were used. The impedance of the EMD/electrolyte interface was also minimized when 5.0 M KOH was used as the electrolyte. This correlates with a maximum in electrolyte conductivity. The electrode impedance also increased as the degree of EMD reduction was increased, as was expected. Under these experimental conditions the electrode impedance increased in the presence of TiO_2 (anatase), which has negative implications for its commercial use. This conclusion was reached despite the differences in experimental conditions between this work and in commercial applications. An equivalent circuit was also derived and used as an aid in interpreting the impedance data.

1. Introduction

Manganese dioxide is the most common positive electrode materials used in portable power sources. Its widespread use is a direct result of a unique combination of its electrochemical, chemical and economic properties [1], including (i) its ability to sustain relatively high discharge rates for prolonged periods of time; (ii) an abundance of the raw materials necessary for synthesis; and (iii) the low cost of production, despite the fact that production of primary alkaline Zn–MnO_2 cells may require up to 10 times the energy of its expected output. Commercial alkaline Zn–MnO_2 cells are predominantly limited to primary applications; however, in recent years a rechargeable alkaline Zn–MnO_2 cell has been developed and marketed [2].

The power generation reaction the manganese dioxide cathode undergoes is

$$MnOOH_r + \Delta H_2O + \Delta e^- \leftrightarrow MnOOH_{r+\Delta} + \Delta OH^- \quad (1)$$

where $0 \leqslant (r + \Delta) \leqslant 1$. Equation 1 represents a homogeneous, solid solution process involving proton and electron insertion through the manganese dioxide-electrolyte interface, into the manganese dioxide structure. Once inserted, the protons and electrons diffuse away from the surface, into the bulk of the manganese dioxide [3–11]. Equation 1 represents the manganese dioxide reduction mechanism for the majority of the composition range $0 \leqslant (r + \Delta) \leqslant 1$. However, towards the later stages of reduction, when, for example, $(r + \Delta) \geqslant 0.8$, increasing strain within the $MnOOH_{r+\Delta}$ solid solution (due to proton insertion and Mn^{4+} reduction to Mn^{3+}) causes a structural collapse to a more stable structure [12]. This stage of the reduction is heterogeneous in nature.

The purpose of this study was to investigate the behaviour of the manganese dioxide electrode, particularly the manganese dioxide-electrolyte interfacial behaviour, under a wide variety of experimental conditions. Specifically, the effects of (i) electrode thickness; (ii) electrode compaction pressure; (iii) manganese dioxide oxidation state; (iv) electrolyte concentration; (v) electrolyte availability; and (vi) the presence of additives (TiO_2 (anatase)) were investigated. While (i)–(v) are standard electrode variables, the presence of TiO_2 (anatase) in the manganese dioxide cathode has been shown to lead to a service improvement for cells using these cathodes [13–15]. This work will shed light on the role that TiO_2 (anatase) plays in improving manganese dioxide discharge performance.

2. Experimental

2.1. *Manganese dioxide samples*

The starting manganese dioxide sample used in this work was supplied by Eveready Battery Company, Inc. It was prepared by electrolytic deposition onto a titanium anode from a hot, acidic (H_2SO_4) $MnSO_4$ solution (EMD), and had an average composition of $MnO_{1.95}$, as determined using the potentiometric titration method described by Vetter and Jaeger [16].

A partially reduced manganese dioxide (REMD) was prepared by immersing ~10 g of the original EMD in 100 cm^3 of anhydrous 2-propanol at room temperature. After 7 days the suspension was filtered and the solid vacuum dried at room temperature. The REMD sample had an average composition of $MnO_{1.70}$.

2.2. *Electrode preparation and the electrochemical cell*

Electrodes were prepared by thoroughly mixing manganese dioxide either EMD or REMD and electrolyte using a mortar and pestle. Light grinding was used so as not to alter the particle size distribution. Manganese dioxide electrodes used in cells are typically prepared with ~5–10% of graphite to enhance the electrical conductivity of the electrode. However, for this study, graphite was excluded from the blackmix so that our experiments could focus on the interaction between manganese dioxide, electrode additive and the electrolyte.

A schematic diagram of the electrochemical cell is shown in Figure 1. An appropriate amount of blackmix (0.5–3.0 g) was placed between the pistons. The Teflon® and stainless steel sleeves surrounding the electrode were used both to constrain the electrode and to prevent direct electrical contact between the pistons, which also acted as current collectors. The blackmix was then compressed by the pistons to form the pellet electrode. This part of the cell was then mounted between the cover and baseplate using a uniform and constant pressure (0.3 N m torque on each nut).

2.3. *Apparatus*

Impedance spectra were measured between 60 kHz and 0.1 Hz using a Solartron Instruments 1255 Frequency Response Analyzer and 1287 Electrochemical Interface controlled by ZPLOT software. A 5 mV sinusoidal voltage was used and scans were conducted in triplicate to ensure reproducibility.

2.4. *Numerical analysis*

Modelling of experimental EIS data was carried out using complex non-linear least squares regression (CNLS) as described by Boukamp [17, 18]. It involved simultaneously fitting the real and imaginary components of the impedance, predicted from the equivalent circuit, using the expression

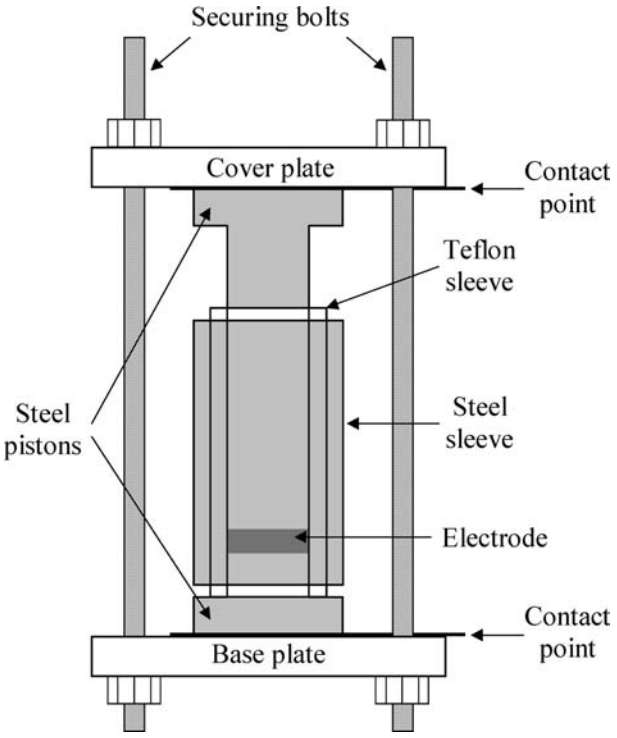

Fig. 1. Schematic diagram of the electrochemical cell.

$$S = \sum_i w_i[\{Z'_i - Z'_i(\omega)\}^2 + \{Z''_i - Z''_i(\omega)\}^2] \quad (2)$$

where S is indicative of the divergence between experimental and predicted data, $Z_i^* = Z'_i + jZ''_i$ is the measured data set, $Z_i^*(\omega) = Z'_i(\omega) + jZ''_i(\omega)$ is the predicted data set, and w_i is a weighting factor inversely proportional the square of the modulus of the measured data set; i.e.,

$$w_i = \frac{1}{|Z_i^*|^2} \quad (3)$$

The fitting procedure involved optimizing the equivalent circuit parameters such that S is minimized.

3. Results and discussion

3.1. *Physicochemical processes and electrical equivalent circuits*

The equivalent circuit for the manganese dioxide electrode system must be based on a physical picture of the electrode [19]. On a microscopic scale the electrode is composed of randomly oriented manganese dioxide particles, with electrolyte filling the interstitial spaces between the particles. Manganese dioxide is very porous (BET surface area 10–100 $m^2\ g^{-1}$), so we also expect electrolyte to be present in these pores. The assumptions

are that there is a continuous path of manganese dioxide and electrolyte between the current collectors, and that the interstitial spaces within the electrode are filled with electrolyte. This depends on the conditions under which the electrode was prepared; e.g., in an electrode with a relatively high proportion of electrolyte, all interstitial and pore spaces are filled and each manganese dioxide particle is covered with electrolyte, thus inhibiting electronic conduction through the electrode. Alternatively, in a relatively dry electrode, the ionic conduction path is limited. Assuming that both conduction paths are present, they will operate in parallel.

3.1.1. *Current collector/electrode interface*
At this interface charge transfer can occur between the stainless steel current collector and either the manganese dioxide or electrolyte. The contact between current collector and manganese dioxide is assumed to be electronic and of low resistance. Given the small sinusoidal perturbation used here (5 mV RMS), no faradaic charge transfer can occur between the current collector and the electrolyte. However, a non-faradaic double-layer capacitance can be established. Charge transfer from the current collector to the manganese dioxide and electrolyte occur in parallel.

3.1.2. *Bulk manganese dioxide*
Charge transport here is entirely electronic (R_M). The impact of inter-particle contacts is determined by electrode preparation. With a relatively high proportion of electrolyte, electronic conduction between particles would be inhibited by the electrolyte coating each particle; i.e., electronic to ionic charge transfer has to occur. Conversely, when there is a lack of electrolyte, charge transport through the electrode may be entirely electronic.

3.1.3. *Bulk electrolyte*
With a small AC signal no faradaic charge transfer reactions can occur between the current collector and the electrolyte. Nevertheless, non-faradaic double-layer charging at the current collector–electrolyte interface can be represented by a capacitance (C^*_{DL}). Charge transport along the tortuous electrolyte path is entirely ionic, and can be represented by a resistance (R_E).

3.1.4. *Manganese dioxide-electrolyte interface*
With only manganese dioxide and electrolyte present in the cell, charge transfer at this interface depends on both the forward and reverse reactions in Equation 1. The sinusoidal voltage applied to the cell ensures different potentials within the electrode, although no net charge transfer occurs. Hence, those regions within the electrode at relatively negative potentials will be reduced, and correspondingly those at more positive potentials will be oxidized.

In terms of equivalent circuit elements, the faradaic processes at this interface can be represented by the series arrangement of a charge transfer resistance for proton insertion or extraction (R_{CT}), and an impedance to mass transport in the manganese dioxide or electrolyte [20]. The use of a Warburg impedance (diffusion limited with semi-infinite boundary conditions [21, 22]) is questionable due to the porous nature of manganese dioxide, meaning that diffusion fronts will likely meet within the solid. Therefore, we propose to use a general constant phase angle impedance (Z_{CPE}) [23, 24]; i.e.,

$$Z_{CPE} = \sigma\omega^{-m}\left\{\cos\left(\frac{m\pi}{2}\right) - j\sin\left(\frac{m\pi}{2}\right)\right\} \quad (0 < m < 1) \tag{4}$$

where σ and m are the CPE pre-factor and exponent, respectively.

For a smooth planar electrode, non-faradaic charging of the electrode surface gives rise to the classical double-layer capacitance (C_{DL}). However, for rough or porous electrodes, in which the AC signal penetration is comparable to the depth of the pores, an ionic current is developed within the pores that opposes the electronic current within the solid, leading to a situation best interpreted by a RC transmission line [25]. A semi-infinite, uniform RC transmission line can be represented by a Warburg impedance. However, for rough and porous electrodes, the RC transmission line is non-uniform and so a more general constant phase angle impedance is required (Z'_{CPE}; Equation 4). Therefore, the non-faradaic processes that occur can be represented by the series arrangement of C_{DL} and Z'_{CPE}. This representation has been used previously to describe the impedance behaviour of the Li_xCoO_2 [26] and Li_xTiS_2 [20] electrodes, which are solid state ion insertion electrodes similar to manganese dioxide. The equivalent circuit for the interface can therefore be represented by the parallel arrangement of the faradaic and non-faradaic circuit elements (Randles-type circuit [22]).

Essentially, there are three charge transport paths operating in parallel through the electrode; i.e., (i) a electronic path through the manganese dioxide particles (R_M); (ii) an ionic path through the electrolyte (R_E and C^*_{DL}); and (iii) a charge transfer path involving the manganese dioxide/electrolyte interface. An additional resistance (R) is in series with the interfacial impedance to take into consideration charge transport in either the solid or electrolyte before an after transfer. The resultant equivalent circuit for the manganese dioxide electrode is shown in Figure 2a.

3.2. *Modelling of the experimental impedance data*

A typical example (Nyquist plot) of the impedance response of the manganese dioxide electrode (60 kHz to 0.1 Hz) is shown in Figure 3. The data in this figure is for an EMD electrode containing ~10% (w/w) 9 M KOH as the electrolyte, compressed under 2.3×10^3 kg. In this frequency range (60 kHz to 0.6 Hz) the impedance consists of a very depressed and distorted semi-circular arc. Distortion of the semi-circle, particularly at

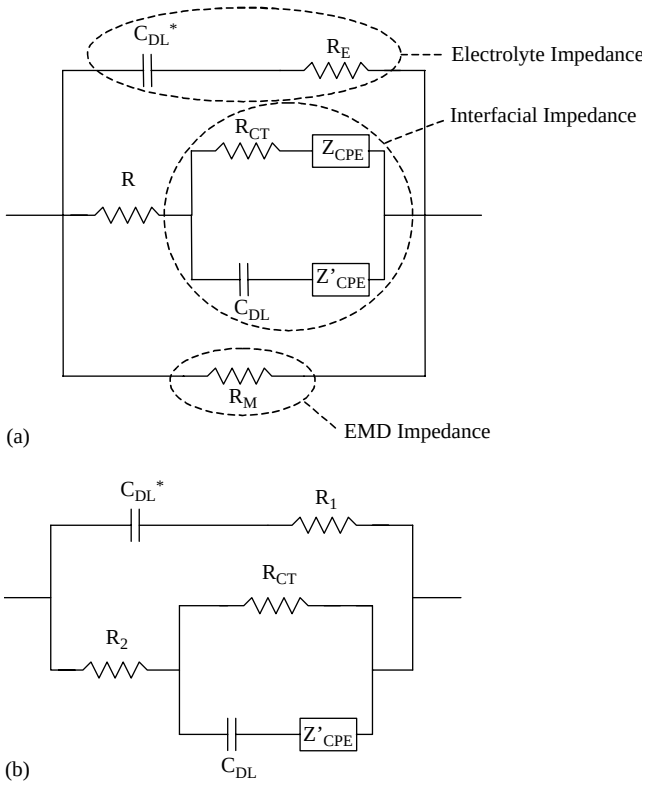

Fig. 2. (a) Original and (b) simplified equivalent circuit.

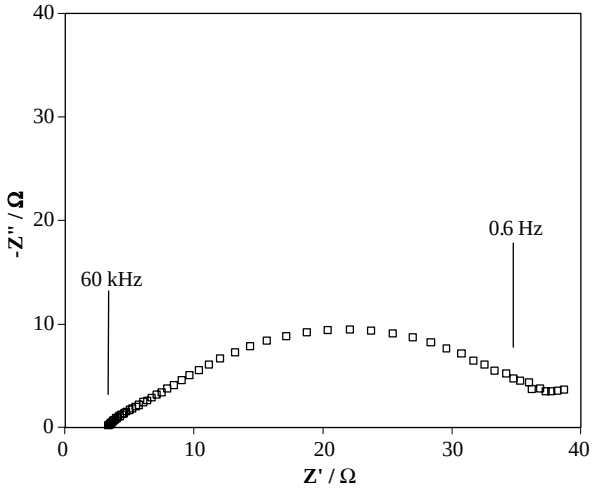

Fig. 3. Typical impedance response for EMD: 6. ~10% 9 M KOH; compaction pressure 2.3×10^3 kg; electrode thickness 0.200 cm; frequency range 60 kHz to 0.1 Hz.

high frequencies, may be due to the presence of another overlapping semi-circle. At a frequency of 0.6 Hz the imaginary component of the impedance begins to increase, most probably due to diffusional processes within the electrode. In subsequent Nyquist plots, the $-Z''$ axis will be expanded so that any trends in the data will be more evident.

The experimental EIS data were then modelled to the equivalent circuit (Figure 2a) using the CNLS technique. From this it became apparent that a number of simplifications to the equivalent circuit could be made (Table 1). R_M can be omitted since it made essentially no change to the parameters or the sum of squares of the residuals (SSR). Furthermore, it was found that m tended towards zero in this and other series of impedance data. The relatively narrow frequency range used here precludes its inclusion and significance in the equivalent circuit, and so m was set equal to zero, meaning the interfacial impedance is a pure resistance. The resultant simplified equivalent circuit is shown in Figure 2b. R_1 and R_2 take into consideration the effect that R_M has on R_E and R, respectively. A comparison between experimental and predicted impedance data is shown in Figure 4. The divergence was minimal ($< \pm 2\%$) over the frequency range studied.

3.3. *Electrode variables*

3.3.1. *Electrode thickness*

The relationship between impedance and electrode thickness was determined for all electrodes examined in this study. As shown in Figure 5, increasing the electrode thickness increases the overall impedance. This is also reflected in the equivalent circuit parameters (Table 2a).

R_1, R_{CT}, R_2 and C_{DL} have intrinsic values that are functions of either electrode thickness or interfacial area. Increasing the electrode thickness proportionately increases the EMD/electrolyte interfacial area. Therefore, R_1, R_2 and R_{CT} should increase, and C_{DL} should decrease. Determining intrinsic equivalent circuit parameters from this data is difficult due to the tortuosity of the electrolyte path, and also because of our uncertainty associated with the electrochemically active surface area of EMD. To elaborate further, conventional methods of measuring surface area (e.g., BET isotherm) require extreme sample pre-treatment which degrades EMD performance. Furthermore, the typical adsorbate (N_2) is very different to the adsorbed electrolyte species present in aqueous systems (H_2O).

Changes in impedance with electrode thickness also allow for determination of electrode resistivity, as well

Table 1. Equivalent circuit parameters during equivalent circuit development

	R_M /Ω	R_E /Ω	C^*_{DL} /μF	R_{CT} /Ω	σ /Ω s^{-m}	m	C_{DL} /μF	σ' /Ω $s^{-m'}$	m'	R /Ω	SSR
Original	15,400	26.4	1.03	14.2	19.2	0.134	815	115	0.432	3.7	0.003
#1	–	26.4	1.03	14.2	19.1	0.134	815	115	0.432	3.7	0.003
#2	–	21.6	1.11	30.2	0	0	1740	144	0.472	4.0	0.006

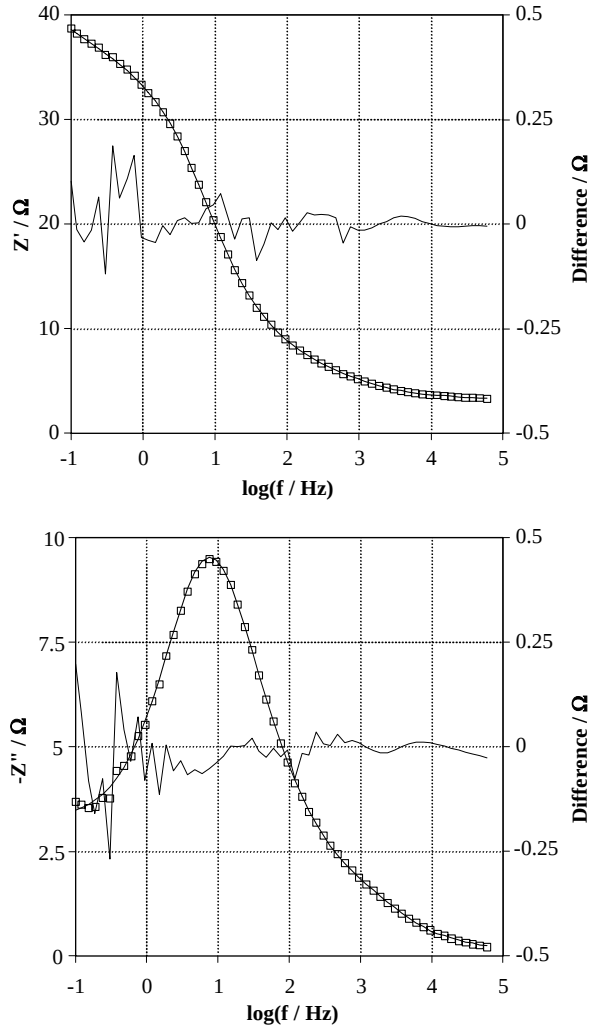

Fig. 4. Comparison between predicted and experimental impedance data: EMD + ~10% 9 M KOH; compaction pressure 2.3×10^3 kg; electrode thickness 0.200 cm; frequency range 60 kHz to 0.1 Hz.

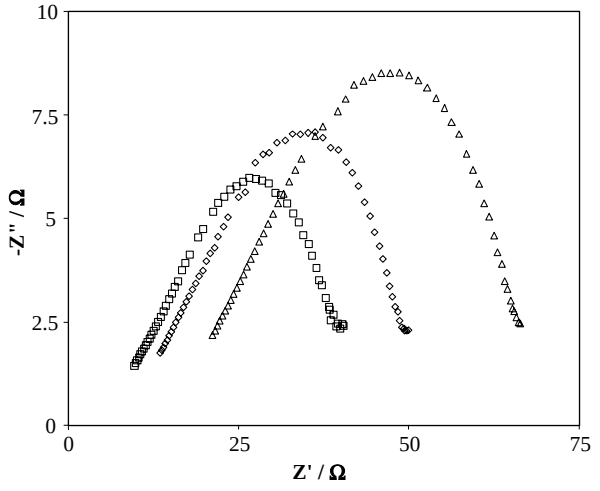

Fig. 5. Typical effects of electrode thickness on the impedance of EMD: ~5% 9 M KOH; compaction pressure 2.3×10^3 kg; frequency range 60 kHz to 0.1 Hz. (□) 0.107 cm; (◇) 0.179 cm; (△) 0.331 cm.

as any interfacial resistance between the current collectors and the electrode. At high frequencies, capacitor and constant phase angle element impedance tends to zero, implying a pure resistance. Therefore, using the fitted equivalent circuit parameters, the high frequency intercept with the Z' axis (Z'_{HI}) is

$$Z'_{HI} = \frac{R_1 R_2}{R_1 + R_2} \tag{5}$$

and then expressed as a function of electrode thickness (l) [27]; i.e.,

$$Z'_{HI} = \rho \frac{l}{A} + R_C \tag{6}$$

where ρ is electrode resistivity (Ω cm), A is electrode area (cm^2) and R_C is the current collector–electrode contact resistance (Ω). Plotting Z'_{HI} vs l gives a straight line with slope ρ/A and intercept R_C. With an electrode area of 1.27 cm^2, ρ was determined to be ~60 Ω cm, while R_C was ~2 Ω. This is consistent with the data reported previously by Xia et al. (~10^2 Ω cm) [28], the variation being explained by a different compaction pressure and EMD oxidation state.

3.3.2. *Electrode compaction pressure*

The effects of compaction pressure on electrode impedance are shown in Figure 6, while the calculated equivalent circuit parameters are shown in Table 2b. This EIS data is based on a 0.200 cm thick electrodes, interpolated from the available data. Clearly as the compaction pressure was increased, the overall electrode impedance decreased.

The compaction pressure effects the void space, and hence the electronic and ionic conduction paths through the electrode. At low compaction pressures, it is possible that there are unfilled void spaces within the electrode. These are essentially barriers to both ionic and electronic conduction, and hence increase electrode impedance. Increasing the compaction pressure progressively removes these voids, thus making a more complete ionic and electronic path through the electrode. This is consistent with the observed decrease in R_1 and R_2.

At low compaction pressures, the thin film of electrolyte surrounding each EMD particle would inhibit electronic conduction. However, as the pressure is increased, electrolyte between particles is forced away, thus bringing the EMD particles into closer contact, hence lowering the inter-particle resistance (decreasing R_2). The electrolyte pushed away from the grain boundaries would aid in filling the void spaces within the electrode, thus enhancing the electrolyte connectivity through the electrode (decrease R_1). It has been shown that, in the absence of electrolyte, the EMD grain boundary resistance decreases as the compaction pressure increases [29], further contributing to lowering R_2.

At the EMD/electrolyte interface a possible scenario is that increasing the compaction pressure forces electrolyte further into EMD pores, to a depth unattainable

Table 2. Calculated equivalent circuit parameters

Variable		R_1 /Ω	C^*_{DL} /μF	R_{CT} /Ω	C_{DL} /μF	σ' /Ω $s^{-m'}$	m'	R_2 /Ω	ρ /Ω cm	R_C /Ω	τ
(a) Thickness (/cm)	0.107	63.9	0.058	30.0	1440	263	0.407	9.7			
	0.179	122.9	0.030	36.0	869	309	0.393	13.0			
	0.331	261.2	0.015	45.3	845	419	0.395	20.4			
(b) Pressure (/10^3 kg)	0	847.5	0.007	66.2	393	780	0.358	19.4	89.1	4.7	
	0.5	289.3	0.011	52.7	445	538	0.375	14.4	68.1	2.7	
	1.4	188.9	0.016	39.9	517	374	0.377	13.2	61.9	2.6	
	2.3	166.4	0.019	37.2	576	303	0.375	13.4	59.9	3.1	
(c) Electrolyte (/%)	0								444.0	1.5	
	1.37	2986	6×10^{-4}	125.1	6	7×10^{-4}	0.291	0			308
	1.94	2118	1×10^{-3}	108.5	22	2×10^{-4}	0.216	0			316
	4.79	149.5	0.029	55.3	659	353	0.348	16.9	140.1	4.8	4.8
	9.97	20.6	1.150	30.5	1950	153	0.482	4.1	18.6	0.4	10.0
(d) [KOH] (/M)	1	121.2	0.046	40.0	1060	270	0.391	8.7	45.0	1.0	
	3	92.5	0.085	36.7	955	289	0.403	8.2	47.9	0.3	
	5	65.4	0.198	27.4	1520	99	0.369	5.7	29.8	0.7	
	7	47.2	0.487	29.8	1500	151	0.432	4.6	38.0	1.6	
	9	20.6	1.150	30.5	1950	153	0.482	4.1	18.6	0.4	
(e) x in MnO_x	1.95	149.5	0.029	55.3	659	353	0.348	16.9	140.1	4.8	
	1.70	506.8	0.029	136.8	1350	226	0.353	42.0	192.3	5.5	
(f) EMD + TiO_2 (anatase) (/%)	0	139.0	0.028	37.6	883	330	0.395	14.1	63.7	3.4	
	1.903	140.5	0.051	55.6	914	373	0.395	14.2	65.1	3.3	
REMD + TiO_2 (anatase) (/%)	0	506.8	0.029	136.8	1350	226	0.353	42.0	192.3	5.5	
	1.899	754.6	0.028	244.3	1420	278	0.353	46.3	219.5	6.0	

Standard conditions: EMD, 0.200 cm thick, ~5% 9 M KOH, compaction pressure 2.3×10^3 kg, frequency range 60 kHz–0.1 Hz.

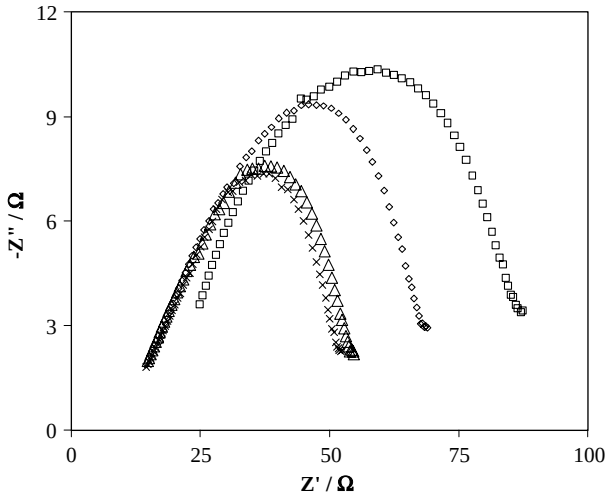

Fig. 6. Typical effects of compaction pressure on the impedance of EMD: ~5% 9 M KOH; electrode thickness 0.200 cm; frequency range 60 kHz to 0.1 Hz. (□) 0 kg; (◇) 0.5×10^3 kg; (△) 1.4×10^3 kg; (×) 2.3×10^3 kg.

by capillary action. The resultant effect is an increase in the EMD/electrolyte interface, causing an increase in R_{CT} and a decrease in C_{DL}. An alternative scenario is that increasing the compaction pressure causes the EMD pore structure to collapse, thus forcing electrolyte out of the pores and into the void space. This would lower the EMD/electrolyte interfacial area resulting in a decrease in R_{CT} and an increase in C_{DL}, as observed in Table 2b. The majority of EMD surface area is associated with pores and so if the total pore structure were to collapse, a much larger change in R_{CT} and C_{DL} should have been observed, suggesting that only a partial collapse occurred. Electrolyte in the pores may have provided some mechanical resistance to pore collapse.

Figure 6 also shows that the EMD electrode impedance tends towards a minimum value. As above, increasing the compaction pressure progressively removes all void spaces within the electrode. A compaction pressure must be reached where there are no void spaces remaining and at this point the EMD/electrolyte interfacial area will have reached its optimum for minimum impedance. It is presumed that at this compaction pressure the EMD inter-particle resistance will also be minimized.

The data in Figure 6 is for an electrode containing a relatively low amount of electrolyte (~5%). However, as the electrolyte content was increased, the changes in the electrode impedance with compaction pressure were much less. With more electrolyte, the void spaces would be removed at lower compaction pressures because there is more electrolyte present to occupy these spaces.

3.3.3. *Electrolyte content*

The effects of electrolyte content on EMD electrode impedance are shown in Figure 7, while the corresponding calculate equivalent circuit parameters are shown in Table 2c. This figure shows the impedance passing through a maximum as the electrolyte content is

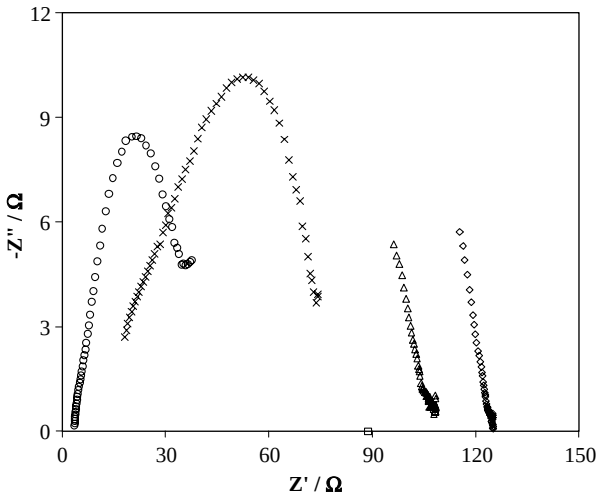

Fig. 7. Effect of electrolyte availability on the impedance of EMD: 9 M KOH; electrode thickness 0.200 cm; compaction pressure 2.3×10^3 kg; frequency range 60 kHz to 0.1 Hz. (□) 0%; (◇) 1.37%; (△) 1.94%; (×) 4.79%; (○) 9.97%.

increased. The zero values of R_2 for low electrolyte electrodes indicate that the EMD/electrolyte interfacial impedance is a pure resistance, and that R_2 was not necessary in the equivalent circuit since it was incorporated into the interfacial impedance. Unfortunately, with $R_2 = 0$ an electrode resistivity could not be calculated for these electrodes.

This figure also emphasizes the importance of the electrolyte conduction path and the EMD/electrolyte interface in determining the electrode impedance. At low electrolyte levels (upto 2%) the electrode impedance increased. Here, R_1 is large since there is very little electrolyte for a conduction path, implying purely electronic conduction. Under such conditions, the electrolyte that is present would be contained in pores and as a thin film on the EMD surface, thus inhibiting the electronic conduction path and raising the impedance. The effect of low electrolyte levels on the EMD/electrolyte interfacial impedance is reflected in the relatively small value of C_{DL}, which can be used as an indicator of the EMD/electrolyte interfacial area.

The maximum impedance corresponds to the point just prior to the formation of a complete ionic conduction path. After this point the electrolyte fully occupies the EMD pores and completely coats the surface of the EMD particles, thus providing an ionic conduction path. The impedance decreases after this point since another, more conductive, charge transfer path has been formed. Further electrolyte addition fills any remaining void spaces in the electrode, therefore decreasing the tortuosity of the electrolyte path and hence decreasing the electrode impedance (KOH electrolytes are more conductive than EMD [28, 30]). Electrolyte tortuosity (τ) can be quantified using

$$\tau = \frac{\rho_a}{\rho_c} \tag{7}$$

where ρ_a and ρ_c are the actual and calculated electrolyte path resistivities. Calculated τ values are shown in Table 2c. The tortuosity factor indicates the apparent electrolyte path length through the electrode, and $\tau \rightarrow 1$ as the electrolyte content is increased.

3.3.4. *Electrolyte concentration*

The effects of electrolyte concentration on the impedance are shown in Figure 8a, while the equivalent circuit parameters for this data are shown in Table 2d. Interpretation of this impedance data is not straightforward, since the electrolyte concentration can influence electrode behaviour in a number of ways. Firstly, the conductivity of aqueous KOH solutions has a maximum of $\sim$0.55 S cm^{-1} at $\sim$6 M KOH [30]. Therefore, R_1 should pass through a minimum as the electrolyte concentration is increased. However, R_1 decreased with increasing KOH concentration, possibly due to R_1 containing contributions from both R_E and R_M, in which case, R_M may be significant.

KOH concentration may also affect the EMD/electrolyte interface. To examine this, R_{CT}, C_{DL} and Z_{CPE}'

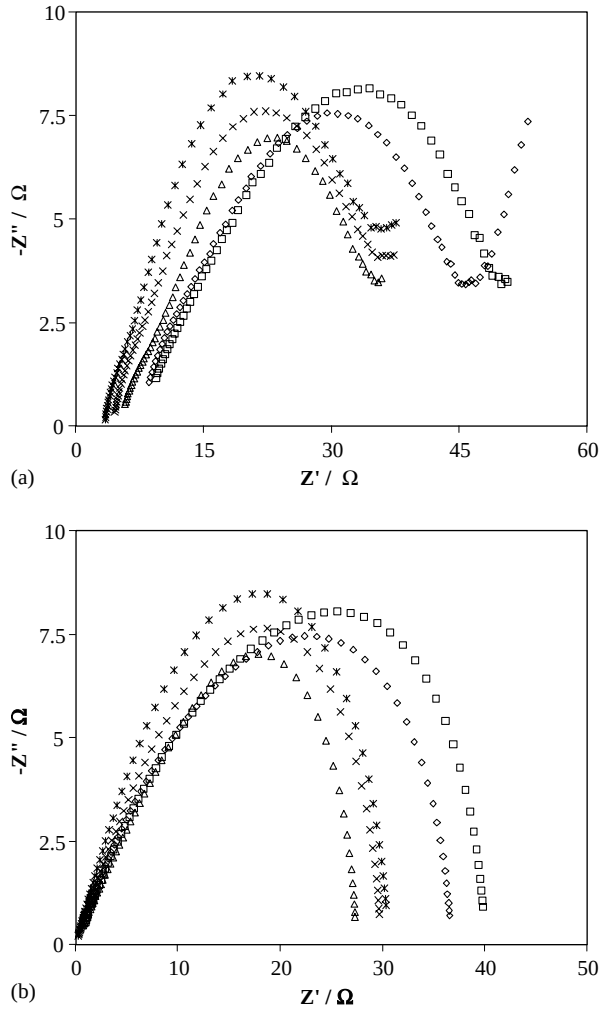

Fig. 8. Effect of electrolyte concentration on the (a) overall impedance and (b) interfacial impedance of EMD: $\sim$10% electrolyte; compaction pressure 2.3×10^3 kg; electrode thickness 0.200 cm; frequency range 60 kHz to 0.1 Hz. (□) 1 M; (◇) 3 M; (△) 5 M; (×) 7 M; (*) 9 M KOH.

were used to generate the interfacial component of the impedance, as shown in Figure 8b. There is a clear correlation between interfacial impedance and electrolyte conductivity, with the lowest interfacial impedance corresponding to the highest conductivity electrolyte. This results from the double-layer structure at the interface and the amount of 'free' water molecules available for charge transfer reactions.

This result also has implications on the performance of manganese dioxide in alkaline cathodes. Discharge efficiency is dependent on the rate of reduction and the rate at which reduced species can diffuse away from the particle surface. From before, there is an optimum electrolyte concentration where the manganese dioxide redox processes are the most facile. The exchange current (I_0) under these conditions, calculated using [31]

$$I_0 = \frac{RT}{nFR_{CT}} \tag{8}$$

where R is the gas constant, T is the temperature, n is the number of electrons involved in the redox process and F is Faraday's constant, was found to be 9.4×10^{-4} A with 5 M KOH as the electrolyte.

3.3.5. *EMD oxidation state*

A typical example showing the effect of EMD oxidation state is shown in Figure 9. The impedance of the partially reduced EMD shows two distinct depressed semi-circles, suggesting two different processes, each with a different frequency dependency. If similar processes are occurring in the unreduced EMD sample, then reduction causes a change in the frequency dependence of these processes. This figure shows that as EMD oxidation state is lowered, the impedance increases dramatically, as reflected in the equivalent circuit parameters in Table 2e.

The degree of EMD reduction has been reported previously [28] to have a significant effect on the solid phase conductivity. These authors reported the conductivity to decrease from $\sim 10^{-2}$ S cm^{-1} at a composition of $MnO_{1.95}$, to $\sim 10^{-7}$ S cm^{-1} at a composition of $MnO_{1.55}$. The consequences of this decrease in electronic conductivity would be an increase in the value of R_M, or in this work, R_1 and R_2, as was observed.

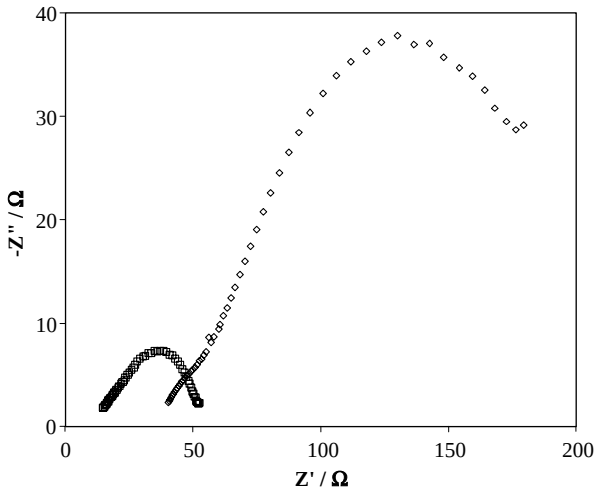

Fig. 9. Effect of EMD oxidation state on the impedance: ~5% 9 M KOH; compaction pressure 2.3×10^3 kg; electrode thickness 0.200 cm; frequency range 60 kHz to 0.1 Hz. (□) EMD ($\sim MnO_{1.95}$); (◇) reduced EMD ($\sim MnO_{1.70}$).

Oxidation state also has an effect on the EMD/electrolyte interfacial properties. During homogeneous EMD reduction, there must be sites available in the EMD structure for the inserted protons and electrons to be located (Equation 1). In partially reduced EMD, a fraction of the insertion sites are already occupied. Consequently, R_{CT} should be larger for a partially reduced EMD compared to an unreduced EMD simply because access to insertion sites is somewhat limited. Furthermore, because of an increased R_{CT}, more charge should be associated with double-layer formation. Therefore, an increase in C_{DL} was expected to occur as the EMD was reduced.

The implications of this behaviour for commercial EMD electrodes are that as reduction proceeds, proton and electron insertion becomes less facile. Eventually an electrode composition is reached where homogeneous reduction is kinetically unfavourable, thus signifying the end of useful life. Secondly, increasing the degree of EMD reduction leads to an increase in EMD resistivity, which in turn leads to an increase in the ohmic polarization of the electrode. This again limits the working cathode voltage, and in extreme cases, can cause electrode failure.

3.3.6. *Inclusion of TiO_2 (anatase)*

Figure 10a shows the typical effects of including TiO_2 (anatase) on the impedance of the EMD electrode. At high frequencies there is little difference between the electrodes; however, at lower frequencies the differences become more significant, with the electrode containing TiO_2 (anatase) having a larger impedance. The calculated equivalent circuit parameters (Table 2f) show that including TiO_2 (anatase) in an unreduced EMD electrode ($MnO_{1.95}$) leads to relatively small changes in the physical properties of the electrode (R_1, C^*_{DL} and R_2), while the impedance of the EMD-electrolyte interface was increased (R_{CT}, C_{DL} and Z'_{CPE}). However, it has been reported that the beneficial effects of TiO_2 (anatase) inclusion are only apparent during the latter stages of discharge, when the EMD oxidation state is much lower [13, 14]. Therefore, a similar comparison was made using an electrode with partially reduced EMD ($MnO_{1.70}$). In this case, TiO_2 (anatase) increased the impedance, making it unclear what its inclusion does to improve performance.

The above data suggests that TiO_2 (anatase) inclusion is detrimental for electrode performance. However, these experimental conditions are not representative of battery systems. For instance, the partially reduced EMD was prepared by chemical reduction, and then mixed with TiO_2 (anatase) to form the electrode material. However, commercially, TiO_2 (anatase) would

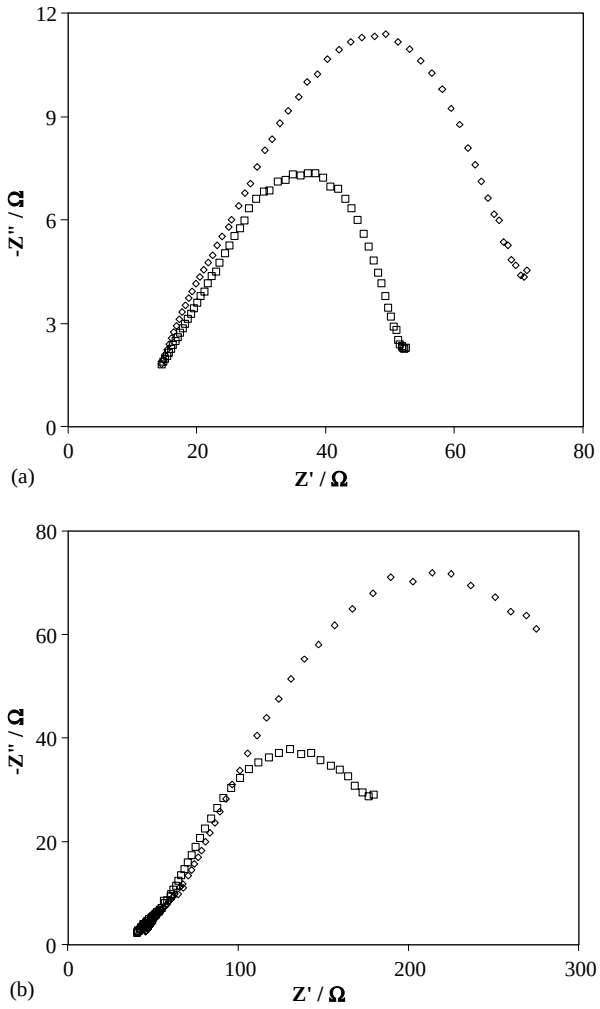

Fig. 10. Effect of TiO_2 (anatase) inclusion on the impedance of EMD: ~5% 9 M KOH; compaction pressure 2.3×10^3 kg; electrode thickness 0.200 cm; frequency range 60 kHz to 0.1 Hz. (a) EMD ($MnO_{1.95}$) + (□) 0% and (◇) 1.90% TiO_2 (anatase); (b) REMD ($MnO_{1.70}$) (□) 0% and (◇) 1.90% TiO_2 (anatase).

be present *in situ* when EMD is being reduced. Therefore, there is the possibility of chemical or physical interaction leading to the observed performance improvements.

Another possibility is that during these EIS experiments measurements were made under quasi-equilibrium conditions. However, the beneficial effects of TiO_2 (anatase) were reported to occur under high discharge rate conditions, with considerable electrode polarization. This implies that TiO_2 (anatase) has a kinetic effect on the EMD electrode. The specific nature of this effect is unknown at this time; however, it may involve either electrolyte management, lowering the electrode overpotential or enhancing diffusional processes.

4. Summary and conclusions

Two-terminal electrochemical impedance spectroscopy has been used to investigate the behaviour of EMD in concentrated KOH electrolytes under a variety of experimental conditions, including electrode thickness and compaction pressure, electrolyte content and concentration, EMD oxidation state and the presence of TiO_2 (anatase) as an additive. The results from these experiments were modelled using an equivalent circuit derived from our understanding of the physical and electrochemical processes occurring within the electrode.

The electrode impedance was lowered by decreasing the electrode thickness, increasing the electrode compaction pressure and increasing the electrolyte content. As expected, the electrode impedance was also less before the EMD was reduced. The effect of KOH electrolyte concentration on electrode impedance was not straightforward. However, it was found that the EMD/electrolyte interfacial impedance (based on the equivalent circuit) was minimized when the most conductive electrolyte was used. Including TiO_2 (anatase) increased the electrode impedance. These results have implications on the behaviour of the alkaline EMD electrode in commercial applications, where electrode performance of the electrode will be enhanced when the electrode impedance is minimized.

Acknowledgements

The authors would like to acknowledge the financial and technical support of Eveready Battery Company, Inc.

References

1. Y.F. Yao, N. Gupta and H.S. Wroblowa, *J. Electroanal. Chem.* **223** (1987) 107.
2. J. Daniel-Ivad and K. Kordesch, *in* P.D. Bennett and S. Gross (Eds), 'Proceedings of the Symposium on Aqueous Batteries' Vol. 96–16, (The Electrochemical Society, Inc., 1996) p. 11.
3. A. Kozawa and J.F. Yeager, *J. Electrochem. Soc.* **112** (1965) 959.
4. A. Kozawa, T. Kalnoki-Kis and J.F. Yeager, *J. Electrochem. Soc.* **113** (1966) 405.
5. A. Kozawa and R.A. Powers, *J. Electrochem. Soc.* **113** (1966) 870.
6. A. Kozawa and R.A. Powers, *Electrochem. Tech.* **5** (1967) 535.
7. A. Kozawa and R.A. Powers, *J. Electrochem. Soc.* **115** (1968) 122.
8. A. Kozawa and J.F. Yeager, *J. Electrochem. Soc.* **115** (1968) 1003.
9. A. Kozawa and R.A. Powers, *J. Chem. Ed.* **49** (1972) 587.
10. D.A.J. Swinkels, K.E. Anthony, P.M. Fredericks and P.R. Osborn, *J. Electroanal. Chem.* **168** (1984) 433.
11. Y. Chabre and J. Pannetier, *Prog. Solid State Chem.* **23** (1995) 1.
12. J. Fitzpatrick and F.L. Tye, *J. Appl. Electrochem.* **21** (1991) 130.
13. J.E. Mieczkowski and S.P. Markfort, U.S. Patent 5,342,712 (1994).
14. J.E. Mieczkowski and M.W. Howard, U.S. Patent 5,516,604 (1996).
15. S.M. Davis, C.P. Haines, A.A. Leef and P.R. Moses, U.S. Patent 5,532,085 (1996).
16. K.J. Vetter and N. Jaeger, *Electrochim. Acta* **11** (1966) 401.
17. B.A. Boukamp, *Solid State Ionics* **18** (1986) 136.
18. B.A. Boukamp, *Solid State Ionics* **20** (1986) 30.
19. D.D. MacDonald, *in* R. Varma and J.R. Selman (Eds),'Techniques for Characterization of Electrodes and Electrochemical Processes', Vol. 11 (J. Wiley and Sons, Inc., 1991).
20. S.R. Narayanan, D.H. Shen, S. Surampudi, A.I. Attia and G. Halpert, *J. Electrochem. Soc.* **140** (1993) 1854.
21. C. Ho, I.D. Rastrick and R.A. Huggins, *J. Electrochem. Soc.* **127** (1980) 343.
22. J.E.B. Randles, *Discuss. Faraday Soc.* **1** (1947) 11.

23. J.R. MacDonald, *Solid State Ionics* **13** (1984) 147.
24. W. Scheider, *J. Phys. Chem.* **79** (1975) 127.
25. R. de Levie, *Electrochim. Acta* **10** (1965) 113.
26. M.G.S.R. Thomas, P.G. Bruce and J.B. Goodenough, *J. Electrochem. Soc.* **132** (1985) 1521.
27. P.W. Atkins, 'Physical Chemistry', (Oxford University Press, Oxford, 4th edn, 1990).
28. X. Xia, H. Li and Z.H. Chen, *J. Electrochem. Soc.* **136** (1989) 266.
29. S.W. Donne; Unpublished results.
30. 'International Critical Tables of Numerical Data, Physics, Chemistry and Technology', (McGraw-Hill Book Co. New York, 1929).
31. A.J. Bard and L.R. Faulkner, 'Electrochemical Methods: Fundamentals and Applications', (John Wiley and Sons, Inc., New York, 1980).